Kinetics of morphological transitions between mesophases*

2001 J. Phys.: Condens. Matter 13 9089

(http://iopscience.iop.org/0953-8984/13/41/304)

INSTITUTE OF PHYSICS PUBLISHING JOURNAL OF PHYSICS: CONDENSED MATTER

J. Phys.: Condens. Matter **13** (2001) 9089–9112 PII: S0953-8984(01)21462-3

Kinetics of morphological transitions between mesophases*

Makiko Nonomura[1] **and Takao Ohta**[2]

[1] Research Institute for Electronic Science, Hokkaido University, Sapporo, 060-0812, Japan
[2] Institute for Nonlinear Sciences and Applied Mathematics, Graduate School of Sciences, Hiroshima University, Higashi-Hiroshima 739-8526, Japan

Received 29 January 2001, in final form 28 February 2001
Published 28 September 2001
Online at stacks.iop.org/JPhysCM/13/9089

Abstract

We investigate the dynamics of morphological transitions between mesoscopic structures on the basis of the model equation for microphase separation of block copolymers. The phase diagram for the modulated structures is obtained by means of the single-wavenumber approximation. In order to study the time evolution of domains, we derive a coupled set of equations for the amplitudes of the modulated structures in the weak-segregation regime. Simulations of the transitions between lamellar and hexagonal structures are carried out in two dimensions and the results are compared with the theory. Simulations in three dimensions are also presented.

1. Introduction

Domain morphology and kinetics of phase separation have been studied for many years both experimentally and theoretically. In microphase separation of block copolymers, the domain growth ceases at a mesoscopic scale causing there to be various mesophases depending on the block ratio and temperature. It is also well known that mesoscopic domain structures similar to those of block copolymers are formed in water–surfactant mixtures.

There have been many experiments and theories designed to clarify the formation of mesophases. Quite recently much attention has been paid to the kinetics of the transitions between different morphological structures. This order–order transition caused by temperature quench has been studied—for instance, between spherical and cylindrical mesoscopic domain structures [1–3] and between BCC and hexagonal close-packed (HCP) structures [4]. Similar experiments have also been carried out on water–surfactant mixtures [5, 6].

The equilibrium theory for mesophases has been developed to derive the phase diagram [7, 8]. A pathway from one ordered structure to another structure has been investigated by evaluating the free-energy landscape [9–11]. Computer simulations of the morphological transitions in three dimensions have been performed by Qi and Wang [12, 13]. However, they

* This paper is dedicated to Professor S-H Chen on the occasion of his sixty fifth birthday. One of the authors (TO) has taken his inspiration for more than two decades from Professor Chen's pioneering experiments on dynamic critical phenomena and complex fluids.

0953-8984/01/419089+24$30.00

are mainly concerned with the structural transitions which occur almost simultaneously and uniformly in the whole system.

The aim of the present paper is to study, both theoretically and by computer simulations, the kinetics of the morphological transitions. The phase diagram and the stability limit for the mesophases are obtained using the single-wavenumber approximation. This is an extension of the theory given in reference [14]. Our main concern is the role of grain boundaries and dislocations for nucleation of new structures after temperature quench and the growth behaviour of new domains in the matrix of the unstable structure. We study the kinetics of growing structures by means of the amplitude equation. Although the amplitude equation has been used in studying the dynamics of periodic patterns far from equilibrium [15], this method has not been applied, to our knowledge, to the kinetics of morphological transitions of mesophases. In reference [16], the kinetics of hexagonal and lamellar structures invading the uniform state has been considered. However, this is not a transition between two ordered structures.

In two dimensions, we shall show the simulation results of morphological transitions between lamellar and hexagonal structures mediated by defects and make a comparison with our theory. In three-dimensional simulations, we study the transitions from BCC structure to hexagonal or to lamellar structures which have not been reported so far. It is also shown that a new bicontinuous structure having a rhombohedral symmetry can exist between lamellar and hexagonal phases. We discuss the relation with the experimentally observed structure [6].

The organization of the paper is as follows. In section 2, we introduce the free-energy functional for diblock copolymers and the kinetic equation. In section 3, we derive the phase diagram for various modulated structures by means of the single-wavenumber approximation. This approximation is justified for lamellar, hexagonal and BCC structures in the weak-segregation limit. It is known both experimentally [17] and theoretically [7] that a bicontinuous structure called a gyroid exists between lamellar and hexagonal phases. However, we do not consider this phase in the present theoretical analysis since this is beyond the single-wavenumber approximation. The kinetics of the transition between a lamellar structure and a hexagonal structure is investigated in section 4. It is pointed out that there are two different kinds of domain boundary in this case. The ratio of the velocities of the domain boundaries is evaluated. In section 5, we present computer simulations of the morphological transition between lamellar and hexagonal structures in two dimensions and make a comparison with the theoretical results. Simulations in three dimensions are described in section 6. A summary and discussion are given in section 7. In the appendix, the effective free energy for a hexagonal structure is derived in terms of the amplitude and the phase for the periodic structure.

2. The kinetic equation for microphase separation

Our model equation for A–B-type diblock copolymers is given by the following time-evolution equation [18]:

$$\frac{\partial \phi}{\partial t} = \nabla^2 \frac{\delta F}{\delta \phi} \tag{1}$$

where $\phi = \phi_A - \phi_B$ with ϕ_A (ϕ_B) the local volume fraction of the A (B) monomers. The incompressibility condition $\phi_A + \phi_B =$ constant has been assumed. The free-energy functional F is given by [19]

$$F = F_{GL} + F_{LR}. \tag{2}$$

The first part is the usual Ginzburg–Landau free energy

$$F_{GL} = \int \mathrm{d}\vec{r} \left[\frac{1}{2} (\vec{\nabla}\phi)^2 + W(\phi) \right] \tag{3}$$

with $W(\phi) = -(\tau/2)\phi^2 + (g/4)\phi^4$. The coefficients τ and g are assumed to be positive. The second part is specific to copolymers and is given by

$$F_{LR} = \frac{\alpha}{2} \int \mathrm{d}\vec{r} \int \mathrm{d}\vec{r}' \, G(\vec{r}, \vec{r}')[\phi(\vec{r}) - \bar{\phi}][\phi(\vec{r}') - \bar{\phi}] \tag{4}$$

where $\bar{\phi}$ is the average of ϕ. The positive constant α depends on the block ratio $f = N_\mathrm{A}/N$ where N_A (N_B) is the molecular weight of the A (B) block and $N = N_\mathrm{A} + N_\mathrm{B}$. The function $G(\vec{r}, \vec{r}')$ is defined through the relation

$$-\nabla^2 G(\vec{r}, \vec{r}') = \delta(\vec{r} - \vec{r}'). \tag{5}$$

The long-range interaction F_{LR} comes from the osmotic incompressibility of diblock copolymers. It is known that the competition between the short-range attractive interaction given by the gradient term in (3) and the long-range repulsive interaction is a general feature for formation of mesophases [20].

In reference [19], we have calculated the equilibrium free energy for the ordered structures in the strong-segregation limit. However, one cannot realize the morphological transition by changing temperature in the strong-segregation limit because the phase boundaries are independent of temperature. Hence, we are here concerned with the weak-segregation case where morphological transitions are achievable by temperature quench. A similar analysis has been made in reference [14] where, however, only lamellar and hexagonal structures were examined.

In the weak-segregation case, we may retain only the fundamental modes of modulation and hence the local volume fraction ϕ can be written as

$$\phi(\vec{r}) = c + A \sum_i [\mathrm{e}^{\mathrm{i}\vec{Q}_i \cdot \vec{r}} + \mathrm{e}^{-\mathrm{i}\vec{Q}_i \cdot \vec{r}}] \tag{6}$$

where $c = \bar{\phi}$. The magnitude $Q = |\vec{Q}_i|$ ($i = 1, 2, \ldots, n$) of the reciprocal-lattice vectors $\vec{Q}_i$ and the amplitude A should be determined. The gyroid structure cannot be represented by the single-wavenumber approximation (6), which is not considered in the present paper.

Substituting (6) into (2) and ignoring the higher harmonics generated by the nonlinear term ϕ^4, one obtains per unit area

$$F(Q, A) = n\Gamma(Q)A^2 + U(A) \tag{7}$$

where

$$\Gamma(Q) = Q^2 - \tau + \frac{\alpha}{Q^2} \tag{8}$$

and $U(A)$ is the part which does not contain Q and its form depends on the modulated structures.

The two unknown constants Q and A are determined by the minimization of $F(Q, A)$:

$$\frac{\partial F}{\partial Q} = \frac{\partial F}{\partial A} = 0. \tag{9}$$

In particular, one obtains $Q^2 = \sqrt{\alpha}$ from (8).

Generally the nonlinear term in the free energy is not local as in (3) but is nonlocal. In this case, the magnitude of the wavenumber is coupled with the amplitude. Such a correction might be important in the disorder–order kinetics. However, we omit the nonlocality in this paper since it is expected to be a secondary effect in the kinetics of the order–order transitions.

3. Stability for modulated structures

When one deals with the dynamics of a morphological transition where a stable new structure is growing in the matrix of a less stable structure, the mode expansion (6) has to be generalized in such a way that the amplitude may depend on space and time:

$$\phi(\vec{r}) = c + \sum_i [A_i(\vec{r}, t)\mathrm{e}^{\mathrm{i}\vec{Q}_i\cdot\vec{r}} + A_i^*(\vec{r}, t)\mathrm{e}^{-\mathrm{i}\vec{Q}_i\cdot\vec{r}}]. \tag{10}$$

Note that the amplitude is generally complex and A^* is the complex conjugate of A. The phase variable is necessary to represent a weak deformation of the structure, i.e., the elastic effect. The effective free energy for a hexagonal structure in terms of the amplitude and the phase will be given in the appendix.

In this section, we examine the various equilibrium structures and their stability. In this case, the amplitude is assumed to be real and independent of space.

3.1. Lamellar versus hexagonal structures

First, we study lamellar and hexagonal structures. The concentration wave can be represented as

$$\phi(\vec{r}) = c + a(t)[\mathrm{e}^{\mathrm{i}\vec{Q}_1\cdot\vec{r}} + \mathrm{e}^{-\mathrm{i}\vec{Q}_1\cdot\vec{r}}] + h(t)\sum_{i=2,3}[\mathrm{e}^{\mathrm{i}\vec{Q}_i\cdot\vec{r}} + \mathrm{e}^{-\mathrm{i}\vec{Q}_i\cdot\vec{r}}] \tag{11}$$

where $\vec{Q}_1 = (Q, 0)$, $\vec{Q}_2 = (-Q/2, \sqrt{3}Q/2)$ and

$$\vec{Q}_1 + \vec{Q}_2 + \vec{Q}_3 = 0. \tag{12}$$

In this subsection, we ignore, without loss of generality, the third component of the reciprocal-lattice vector. When $h = 0$, equation (11) represents a lamellar mesophase, whereas when $a = h$, it represents a hexagonal structure.

Substituting (11) into (1) yields under the single-wavenumber approximation

$$\frac{\mathrm{d}a}{\mathrm{d}t} = -Q^2\Gamma(Q)a - 3gQ^2(c^2a + a^3 + 2ch^2 + 4ah^2) \tag{13}$$

$$\frac{\mathrm{d}h}{\mathrm{d}t} = -Q^2\Gamma(Q)h - 3gQ^2(c^2h + 2a^2h + 3h^3 + 2cah). \tag{14}$$

Note that since $Q^2 = \sqrt{\alpha}$,

$$\Gamma(Q) = 2\sqrt{\alpha} - \tau. \tag{15}$$

The equilibrium lamellar solution is given from equations (13) and (14) by $h = 0$ and $a \equiv a_e$ where a_e is given by

$$a_e^2 = -\frac{\Gamma(Q)}{3g} - c^2. \tag{16}$$

The right-hand side of (16) must be positive. However, it turns out that the lamellar solution becomes unstable before it becomes negative as shown below.

Linearization of equations (13) and (14) around the equilibrium solution $a = a_e$ and $h = 0$ gives us two decoupled equations:

$$\frac{\mathrm{d}\,\delta a}{\mathrm{d}t} = -6ga_e^2Q^2\,\delta a \tag{17}$$

$$\frac{\mathrm{d}\,\delta h}{\mathrm{d}t} = -3ga_eQ^2(a_e + 2c)\,\delta h \tag{18}$$

where δa and δh denote the deviations. For negative values of c, the equilibrium solution is unstable for hexagonal disturbance when $a_e > 2|c|$. Using (16), this is equivalent to

$$\tau < \tau_{LH} \equiv 2\sqrt{\alpha} + 15gc^2. \tag{19}$$

Note that equations (17) and (18) are decoupled. This means that the lamellar domains undergo a varicose-type modulation at the instability point.

The equilibrium hexagonal solution is given from equations (13) and (14) by $a = h \equiv h_e$ where h_e is the larger solution of the equation

$$3g(5h_e^2 + 2ch_e) = -\Gamma(Q) - 3gc^2. \tag{20}$$

It is readily shown from (20) that $h_e > |c|/5$. Small deviations δa and δh around the equilibrium solution obey

$$\frac{\mathrm{d}\,\delta a}{\mathrm{d}t} = -6gh_eQ^2[(-c + h_e)\,\delta a + 2(2h_e + c)\,\delta h] \tag{21}$$

$$\frac{\mathrm{d}\,\delta h}{\mathrm{d}t} = -6gh_eQ^2[(2h_e + c)\,\delta a + 3h_e\,\delta h]. \tag{22}$$

The coefficient matrix has a positive eigenvalue when $h_e > 2|c|$ or $h_e < |c|/5$, the latter of which is excluded by the above condition. Therefore the hexagonal structure is unstable when $h_e > 2|c|$ which is identical with

$$\tau > \tau_{HL} \equiv 2\sqrt{\alpha} + 51gc^2. \tag{23}$$

The eigenfunction at the instability threshold is given by $(\delta a, \delta h) \propto (2, -1)$ and hence one of the three modes becomes dominant post-threshold as is expected.

In order to determine the coexistence line for lamellar and hexagonal structures, one has to evaluate the equilibrium free energy by using the amplitudes a_e and h_e. The equilibrium free energy per area for a lamellar structure is given, from equations (2) and (10) with $a = a_e$ and $h = 0$, by

$$F_L = -\frac{\tau}{2}c^2 + \frac{g}{4}c^4 - \frac{1}{6g}(\Gamma(Q) + 3gc^2)^2 \tag{24}$$

where we have used (16). Similarly, the free energy for a hexagonal structure is obtained as

$$F_H = -\frac{\tau}{2}c^2 + \frac{g}{4}c^4 - 6gch_e^3 - \frac{45}{2}gh_e^4 \tag{25}$$

where (20) has been used. Comparing (24) and (25) and after elementary calculations, one obtains the coexistence line given by

$$\tau = 2\sqrt{\alpha} + \frac{57 + 18\sqrt{6}}{5}gc^2. \tag{26}$$

3.2. Hexagonal versus BCC structures

The smallest reciprocal vectors which characterize a BCC structure are given by

$$\vec{Q}_1 = (1, -1, 0) \qquad \vec{Q}_2 = (0, 1, -1)$$

$$\vec{Q}_3 = (-1, 0, 1) \qquad \vec{Q}_4 = (1, 1, 0)$$

$$\vec{Q}_5 = (0, 1, 1) \qquad \vec{Q}_6 = (Q/\sqrt{2})(1, 0, 1)$$

where the multiplicative factor $Q/\sqrt{2}$ is omitted for simplicity. These are not independent but have the relations

$$\vec{Q}_1 + \vec{Q}_2 + \vec{Q}_3 = 0 \tag{27}$$

$$\vec{Q}_1 = \vec{Q}_6 - \vec{Q}_5 \tag{28}$$

$$\vec{Q}_2 = \vec{Q}_4 - \vec{Q}_6 \tag{29}$$

$$\vec{Q}_3 = \vec{Q}_5 - \vec{Q}_4. \tag{30}$$

Under the single-wavenumber approximation, one may write the concentration wave for a BCC structure as

$$\phi(\vec{r}) = c + \sum_{i=1,2,3} h_i[\mathrm{e}^{\mathrm{i}\vec{Q}_i\cdot\vec{r}} + \mathrm{e}^{-\mathrm{i}\vec{Q}_i\cdot\vec{r}}] + \sum_{i=4,5,6} b_i[\mathrm{e}^{\mathrm{i}\vec{Q}_i\cdot\vec{r}} + \mathrm{e}^{-\mathrm{i}\vec{Q}_i\cdot\vec{r}}] \tag{31}$$

where the amplitudes b_i and h_i are to be determined ($b_i = h_i$ for BCC structure). When $b_i = 0$, equation (31) with $h_1 = h_2 = h_3 = h$ is a representation of a hexagonal structure. In this case, the axis of a cylindrical domain is along the [111] direction.

Substituting (31) with $h_1 = h_2 = h_3 = h$ and $b_4 = b_5 = b_6 = b$ into (1) and retaining the lowest-order couplings, we obtain

$$\frac{\mathrm{d}h}{\mathrm{d}t} = -Q^2\Gamma(Q)h - 3gQ^2(c^2h + 5h^3 + 6hb^2 + 2ch^2 + 2cb^2 + 4hb^2) \tag{32}$$

$$\frac{\mathrm{d}b}{\mathrm{d}t} = -Q^2\Gamma(Q)b - 3gQ^2(c^2b + 5b^3 + 6h^2b + 4cbh + 4h^2b). \tag{33}$$

The equilibrium solution for a BCC structure is given by putting $b = h = b_e \neq 0$ and $\mathrm{d}h/\mathrm{d}t = \mathrm{d}b/\mathrm{d}t = 0$ in equations (32) and (33) where b_e is the solution of the equation

$$\Gamma(Q) + 3g(c^2 + 15b_e^2 + 4cb_e) = 0. \tag{34}$$

There are two solutions for b_e. The stability of the BCC solution can be examined by substituting $h = b_e + \delta h$ and $b = b_e + \delta b$ into equations (32) and (33) and retaining only the linear terms of the deviations δh and δb:

$$\frac{\mathrm{d}\,\delta h}{\mathrm{d}t} = A\,\delta h + B\,\delta b \tag{35}$$

$$\frac{\mathrm{d}\,\delta b}{\mathrm{d}t} = B\,\delta h + A\,\delta b \tag{36}$$

where

$$A = -30gb_e^2Q^2 \tag{37}$$

$$B = -12gb_eQ^2[5b_e + c]. \tag{38}$$

Putting $\delta h, \delta b \propto \mathrm{e}^{\lambda t}$, one obtains

$$\lambda = \lambda_+ \equiv -6gb_eQ^2[15b_e + 2c] \tag{39}$$

$$\lambda = \lambda_- \equiv 6gb_eQ^2[5b_e + 2c] \tag{40}$$

where (34) has been used. For the negative solution of (34), λ_- is always positive since c is chosen to be negative. Therefore one may consider only the positive solution of (34). When $b_e > 0$, it is readily proved that $\lambda_+ < 0$. Thus the instability of BCC structure occurs when $\lambda_- > 0$, that is, $b_e > (2/5)|c|$, from which one obtains the stability limit

$$\tau = \tau_{BH} \equiv 2\sqrt{\alpha} + \frac{27}{5}gc^2. \tag{41}$$

When $\tau > \tau_{BH}$, a BCC structure is linearly unstable for hexagonal disturbance. The eigenfunction at the instability point is given by $(\delta h, \delta b) = (1, -1)$. It is noted that if one puts $\delta h = \delta b$ in (35), only the eigenvalue λ_+ is obtained and hence no instability is predicted.

The stability of the BCC structure compared with the disorder state can be studied by putting $h_1 = b_e + \delta h_1$, $h_2 = h_3 = b_e + \delta h_2$, $b_4 = b_6 = b_e + \delta b_4$ and $b_5 = b_e + \delta b_5$ in the equations for b_i and h_i and linearizing them. After tedious but elementary calculations, one obtains

$$\tau = \tau_{BO} \equiv 2\sqrt{\alpha} + \frac{11}{5} g c^2. \tag{42}$$

When τ is smaller than τ_{BO}, the BCC structure becomes unstable and the uniform state appears.

The stability limit for the hexagonal structure against BCC disturbance can be obtained similarly. The hexagonal solution is the equilibrium solution of (32) and (33) with $b = 0$ and $h \equiv h_e$ which satisfies (20). By putting $b = \delta b$ and $h = h_e + \delta h$ in (32) and (33) one obtains two decoupled equations:

$$\frac{\partial\, \delta h}{\partial t} = (\lambda - 15 g h_e^2 Q^2)\, \delta h \tag{43}$$

$$\frac{\partial\, \delta b}{\partial t} = \lambda\, \delta b \tag{44}$$

where

$$\lambda = -3 g h_e Q^2 (5 h_e + 2c). \tag{45}$$

Here we have used (20). We find that when $h_e < (2/5)|c|$, the hexagonal structure is unstable for BCC disturbance. Using the solution h_e obtained from (20), the instability condition is given by

$$\tau < \tau_{HB} \equiv 2\sqrt{\alpha} + 3 g c^2. \tag{46}$$

Evaluation of the coexistence line for BCC and hexagonal structures is fairly complicated. Substituting (31) with $h_i = b_i = b_e$ into (2), one obtains the equilibrium free energy per unit area for BCC structure:

$$F_{\mathrm{B}} = -\frac{\tau}{2} c^2 + \frac{g}{4} c^4 - 24 g c b_e^3 - 135 g b_e^4. \tag{47}$$

This should be compared with (25) for the hexagonal state. We make an *ansatz* that the coexistence line takes the form

$$-\Gamma(Q) = D g c^2 \tag{48}$$

where the numerical factor D is to be determined. By using (48), the equilibrium amplitudes h_e and b_e are given from (20) and (34), respectively, by

$$h_e = -(3 + \sqrt{15D - 36})\frac{c}{15} \tag{49}$$

$$b_e = -(2 + \sqrt{5D - 11})\frac{c}{15}. \tag{50}$$

Substituting these into (25) and (47) and equating them, we find numerically $D \approx 3.44$. In this way, the coexistence line is given from (48) by

$$\tau \cong 2\sqrt{\alpha} + 3.44 g c^2. \tag{51}$$

In summary, the lamellar structure is stable for

$$\hat{\tau} > 15 c^2 \tag{52}$$

where

$$\hat{\tau} = (\tau - 2\sqrt{\alpha})/g. \tag{53}$$

The hexagonal structure is stable in the region

$$3c^2 < \hat{\tau} < 51c^2. \tag{54}$$

Finally the BCC structure is stable when

$$\frac{11}{5}c^2 < \hat{\tau} < \frac{27}{5}c^2. \tag{55}$$

Note that there are overlapping regions where two different structures are linearly stable. The coexistence line between lamellar and hexagonal structures is given by

$$\hat{\tau} = \frac{57 + 18\sqrt{6}}{5}c^2 \approx 20.22c^2 \tag{56}$$

and the one between hexagonal and BCC structures by

$$\hat{\tau} \cong 3.44c^2. \tag{57}$$

These lines are depicted in the phase diagram shown in figure 1.

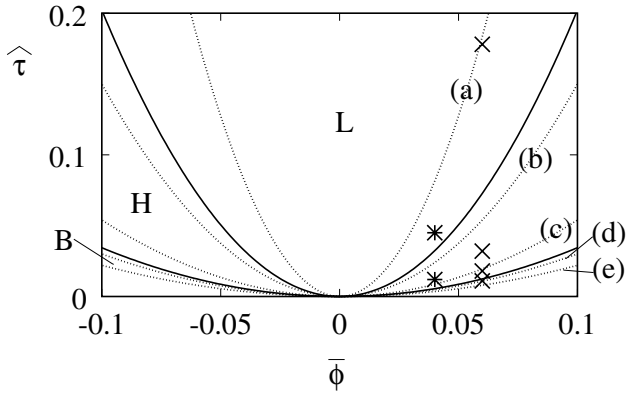

Figure 1. The phase diagram in the weak-segregation regime obtained using the single-wavenumber approximation. The upper solid line is the coexistence line for lamellar and hexagonal structures whereas the lower solid line is the one for hexagonal and BCC structures. The dotted lines (a)–(e) are the stability limits given by equations (52), (54) and (55). The symbol $*$ indicates the parameters $\hat{\tau} = 0.0450$ and 0.0117 for $\bar{\phi} = 0.04$ and the symbol $\times$ indicates $\hat{\tau} = 0.1784$, 0.0317, 0.0184 and 0.0110 for $\bar{\phi} = 0.06$ from the top to the bottom.

4. Kinetics of the lamellar–hexagonal transition

Now we study the kinetics of the morphological transition. We consider the transition from a hexagonal structure to a lamellar structure in the weak-segregation regime with changing temperature. As illustrated in figure 2, there are two different configurations of the domain boundary (interface). In figure 2(a), the interface is parallel to the lamellar stripes whereas that in figure 2(b) makes an angle of $\pi/3$ with the stripes.

When two different mesophases exist, one needs to consider the space dependence of the amplitude in the mode expansion

$$\phi(\vec{r}) = c + 2\sum_{i=1,2,3} H_i(\vec{r}, t)\cos(\vec{Q}_i \cdot \vec{r}). \tag{58}$$

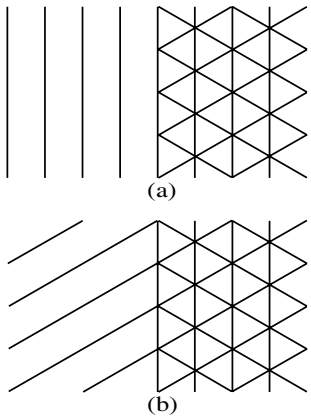

Figure 2. Two kinds of configuration of an interface between lamellar and hexagonal structures: (a) parallel to the lamellar stripes; (b) with the angle $\pi/3$ between the interface and the stripes.

Since the elastic mismatch is expected to be small in the configuration in figure 2, we do not consider the phase variable in (58).

The kinetic equations of the amplitudes H_i are obtained as follows. First we substitute (58) into (1) and then multiply both sides of the equation by $\cos(\vec{Q}_i \cdot \vec{r})$. Next we carry out the integration over one period ignoring the space dependence of H_i. In this way, one obtains

$$\frac{\partial H_1}{\partial t} = 4(\vec{Q}_1 \cdot \vec{\nabla})^2 H_1 + Q_1^2 S_1(H_1, H_2, H_3) + \nabla^2[-\nabla^2 H_1 - S_1(H_1, H_2, H_3)] \tag{59}$$

where

$$S_1 = \tau_{eff} H_1 - 6gcH_2H_3 - 3gH_1^3 - 6gH_1(H_2^2 + H_3^2) \tag{60}$$

with

$$\tau_{eff} = -\Gamma(Q) - 3gc^2 = \tau - 2\sqrt{\alpha} - 3gc^2. \tag{61}$$

Equations for H_2 and H_3 are readily obtained by permutation of the subscripts 1, 2 and 3.

We will ignore the last term of equation (59) in the subsequent analysis. The justification of this approximation requires two conditions. One is the gradient expansion based on the weak spatial variation of the amplitudes. The other is the fact that the equilibrium amplitudes are of the order of $\sqrt{\tau_{eff}}$ when $|c|$ is small. See equations (67) and (68) below. This means that the system is close to the transition point $\tau = 2\sqrt{\alpha}$ and $c = 0$.

Here we make the remark that if fluctuations are taken into account, the transition at $\tau = 2\sqrt{\alpha}$ and $c = 0$ becomes first order [21]. Therefore in order for the above approximation to be valid this fluctuation correction must also be small.

The kinetic equation (59) without the last term can be expressed in an alternative way. In the appendix, we derive the effective free energy in terms of the amplitude and the phase, from which we obtain

$$\frac{\partial H_i}{\partial t} = -Q^2\left[-c_0(\vec{Q}_i \cdot \vec{\nabla})^2 H_i + \frac{\partial G}{\partial H_i}\right] \tag{62}$$

where

$$G = \sum_i \left[-\frac{\tau_{eff}}{2} H_i^2 + \frac{3}{4} g H_i^4\right] + \frac{3g}{2} \sum_{i \neq j} H_i^2 H_j^2 + 6cg H_1 H_2 H_3 \tag{63}$$

with

$$c_0 = \frac{1}{2Q}\frac{\partial}{\partial Q}\frac{1}{Q}\frac{\partial \Gamma(Q)}{\partial Q} = \frac{4\alpha}{Q^6}. \tag{64}$$

Equation (62) agrees precisely with equation (59) without the last term. Note that equation (62) describes a lamellar structure in the special case $H_2 = H_3 = 0$.

The propagating velocity of the interface can be evaluated from equation (62). In particular, we estimate the ratio of the velocity of the interface in figure 2(a) to that in figure 2(b) as follows. In the case of figure 2(a), the reciprocal vectors are given by $\vec{Q}_1 = (1, 0)$, $\vec{Q}_2 = (-1/2, \sqrt{3}/2)$ and $\vec{Q}_3 = (-1/2, -\sqrt{3}/2)$ where the magnitude has been normalized by Q. Since the component $\vec{Q}_1$ represents the lamellar structure in figure 2(a), we write $H_1 = L$. Noting that all of the amplitudes depend only on the x-axis, we have from (62)

$$\frac{\partial L}{\partial t} = c_0 \frac{\partial^2 L}{\partial x^2} - \frac{\partial G}{\partial L} \tag{65}$$

and

$$\frac{\partial H_i}{\partial t} = \frac{c_0}{4}\frac{\partial^2 H_i}{\partial x^2} - \frac{\partial G}{\partial H_i} \tag{66}$$

for $i = 2$ and 3, where the multiplicative factor Q^2 has been eliminated by redefining the unit of time. The boundary conditions are $L = L_{eq}$ and $H_2 = H_3 = 0$ for $x \to -\infty$ and $L = H_2 = H_3 = H_{eq}$ for $x \to \infty$ where

$$L_{eq} = \left(\frac{\tau_{eff}}{3g}\right)^{1/2} \tag{67}$$

and

$$H_{eq} = \frac{-3cg + (9c^2g^2 + 15g\tau_{eff})^{1/2}}{15g} \tag{68}$$

are the uniform equilibrium solutions.

When the interface moves at a constant velocity V_a, the left-hand side of equations (65) and (66) is replaced by $-V_a\,\partial L/\partial x$ and $-V_a\,\partial H_i/\partial x$, respectively. Multiplying these equations by $\partial L/\partial x$ and $\partial H_i/\partial x$ and using the boundary conditions, one obtains

$$V_a = \frac{\Delta G}{\sigma_T} \tag{69}$$

where

$$\Delta G = G(L_{eq}, 0, 0) - G(H_{eq}, H_{eq}, H_{eq}) \tag{70}$$

$$\sigma_T = \int_{-\infty}^{\infty} \mathrm{d}x \left[\left(\frac{\partial L}{\partial x}\right)^2 + \left(\frac{\partial H_2}{\partial x}\right)^2 + \left(\frac{\partial H_3}{\partial x}\right)^2\right]. \tag{71}$$

The numerator ΔG vanishes along the coexistence line.

One obtains the same expression for the interface velocity V_b for the case in figure 2(b). However, since the configuration is different, the numerical coefficients in front of the factor c_0 are different in (65) and (66):

$$\frac{\partial L}{\partial t} = \frac{c_0}{4}\frac{\partial^2 L}{\partial x^2} - \frac{\partial G}{\partial L} \tag{72}$$

$$\frac{\partial H_2}{\partial t} = c_0 \frac{\partial^2 H_2}{\partial x^2} - \frac{\partial G}{\partial H_2} \tag{73}$$

$$\frac{\partial H_3}{\partial t} = \frac{c_0}{4}\frac{\partial^2 H_3}{\partial x^2} - \frac{\partial G}{\partial H_3}. \tag{74}$$

This difference of the coefficients is a geometrical effect arising because the interface normal is not parallel to the reciprocal vectors.

By taking this into account, we estimate σ_T for each configuration in figures 2(a) and 2(b). The interfacial energy in figure 2(a) is estimated from (65) and (66) with the boundary conditions as

$$\sigma_T^a \simeq \frac{(L_{eq} - H_{eq})^2}{\xi_L} + \frac{4H_{eq}^2}{\xi_H} \tag{75}$$

where ξ_L is the interface width for the mode $L(H_1)$ whereas ξ_H is that for H_2 and H_3. Similarly the interfacial energy for the configuration in figure 2(b) is given from (72), (73) and (74) by

$$\sigma_T^b \simeq \frac{2(L_{eq} - H_{eq})^2}{\xi_L} + \frac{3H_{eq}^2}{\xi_H}. \tag{76}$$

In this way, the ratio V_a/V_b is approximately given by

$$\frac{V_a}{V_b} = \frac{\sigma_T^b}{\sigma_T^a} = \frac{2(L_{eq} - H_{eq})^2 + 3H_{eq}^2}{(L_{eq} - H_{eq})^2 + 4H_{eq}^2} \tag{77}$$

where we have used the fact that the intrinsic interface width is the same for both lamellar and hexagonal amplitudes, i.e., $\xi_L = \xi_H$, as was shown in reference [14]. From (26) and (61), one has the relation valid at the coexistence line:

$$\tau_{eff} = \frac{42 + 18\sqrt{6}}{5} g c^2. \tag{78}$$

Substituting this into (67) and (68), the ratio is evaluated as

$$\frac{V_a}{V_b} \approx 0.944. \tag{79}$$

This result will be compared with the simulations in the next section.

5. Computer simulations in two dimensions

Computer simulations of the morphological transitions between lamellar and hexagonal mesophases are shown in figures 3–8 which are obtained by solving equation (1) numerically in two dimensions. The space mesh size is set at 0.7 with the total number of meshes 256×256 and the time increment is 1/45. The periodic boundary conditions are imposed. The coefficients g and α in (2) are fixed as $g = 4.5$ and $\alpha = 0.9$ throughout the simulations.

The domain evolution from a disordered lamellar to a hexagonal structure for $\bar{\phi} = 0.04$ and $\hat{\tau} = 0.0117$ is given in figure 3. This was obtained in such a way that we provide initially a lamellar structure for $\bar{\phi} = 0.04$ and $\hat{\tau} = 0.0450$ and then abruptly change the value of $\hat{\tau}$ to $\hat{\tau} = 0.0117$. One can see that hexagonal domains appear first at the grain boundaries of the lamellar structure having a chevron shape [22] and then gradually cover the whole space.

Shown in figure 4 is the evolution of the hexagonal structure starting from almost perfect lamellar domains. Since we have not introduced the thermal noise in the present kinetic equation (1), there is an incubation time followed by a rather abrupt transition to the hexagonal structure. The time evolution of the scattering intensity is displayed in figure 5. It is clear that when the undulation instability occurs in the stripe domains around $t = 52\,000\,\Delta t$, the hexagonal spots appear in the scattering intensity. The cross-shaped spots here and in figure 8 below are an artifact due to dividing the space into square cells in the numerical simulations.

The transition from disordered hexagons having many grains for $\bar{\phi} = 0.04$ and $\hat{\tau} = 0.0117$ to a lamellar structure for $\bar{\phi} = 0.04$ and $\hat{\tau} = 0.0450$ is shown in figure 6. Again the new

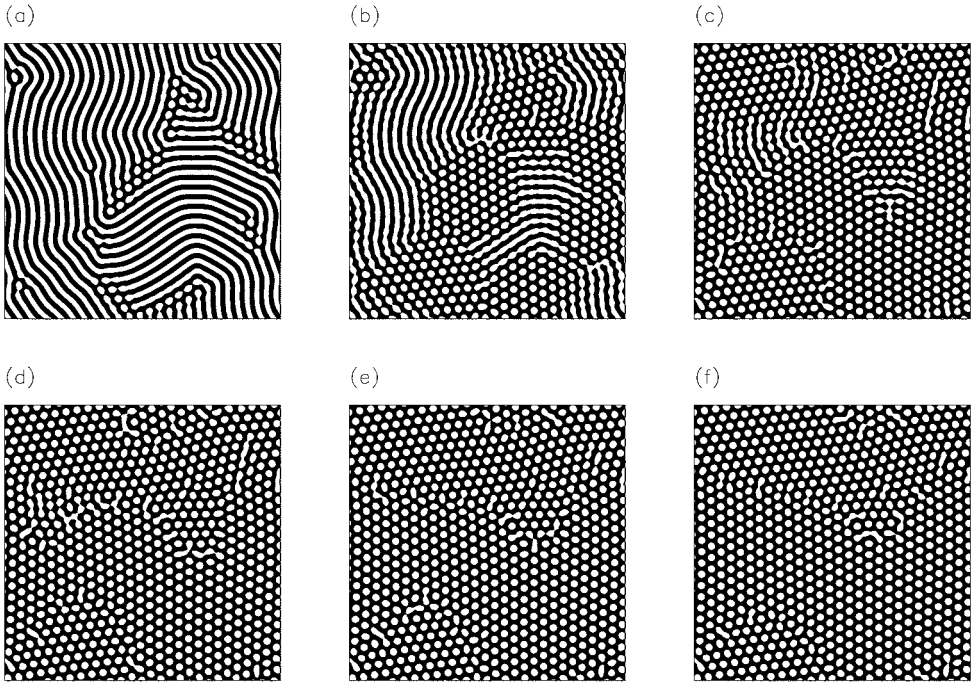

Figure 3. The morphological transition from disordered lamellar to hexagonal structures. The black (white) regions indicate $\phi > (<) \bar{\phi}$. The time is $t = 0$, $10\,000\,\Delta t$, $20\,000\,\Delta t$, $30\,000\,\Delta t$, $40\,000\,\Delta t$ and $50\,000\,\Delta t$ with $\Delta t = 1/45$ from (a) to (f).

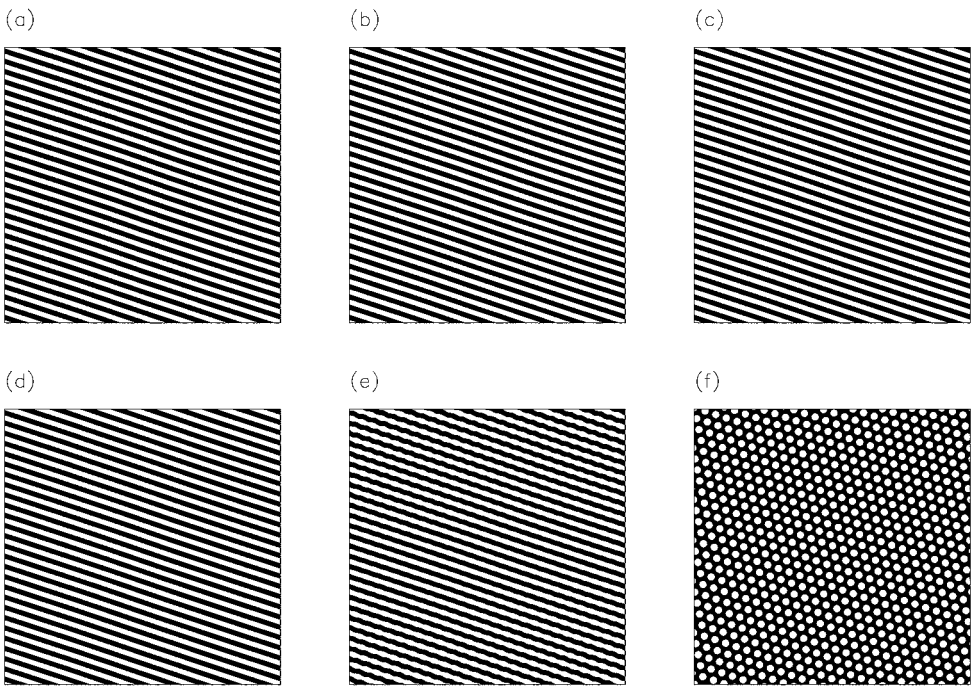

Figure 4. The morphological transition from regular lamellar to hexagonal structures. The time is $t = 0$, $13\,000\,\Delta t$, $26\,000\,\Delta t$, $39\,000\,\Delta t$, $52\,000\,\Delta t$ and $65\,000\,\Delta t$ with $\Delta t = 1/45$ from (a) to (f).

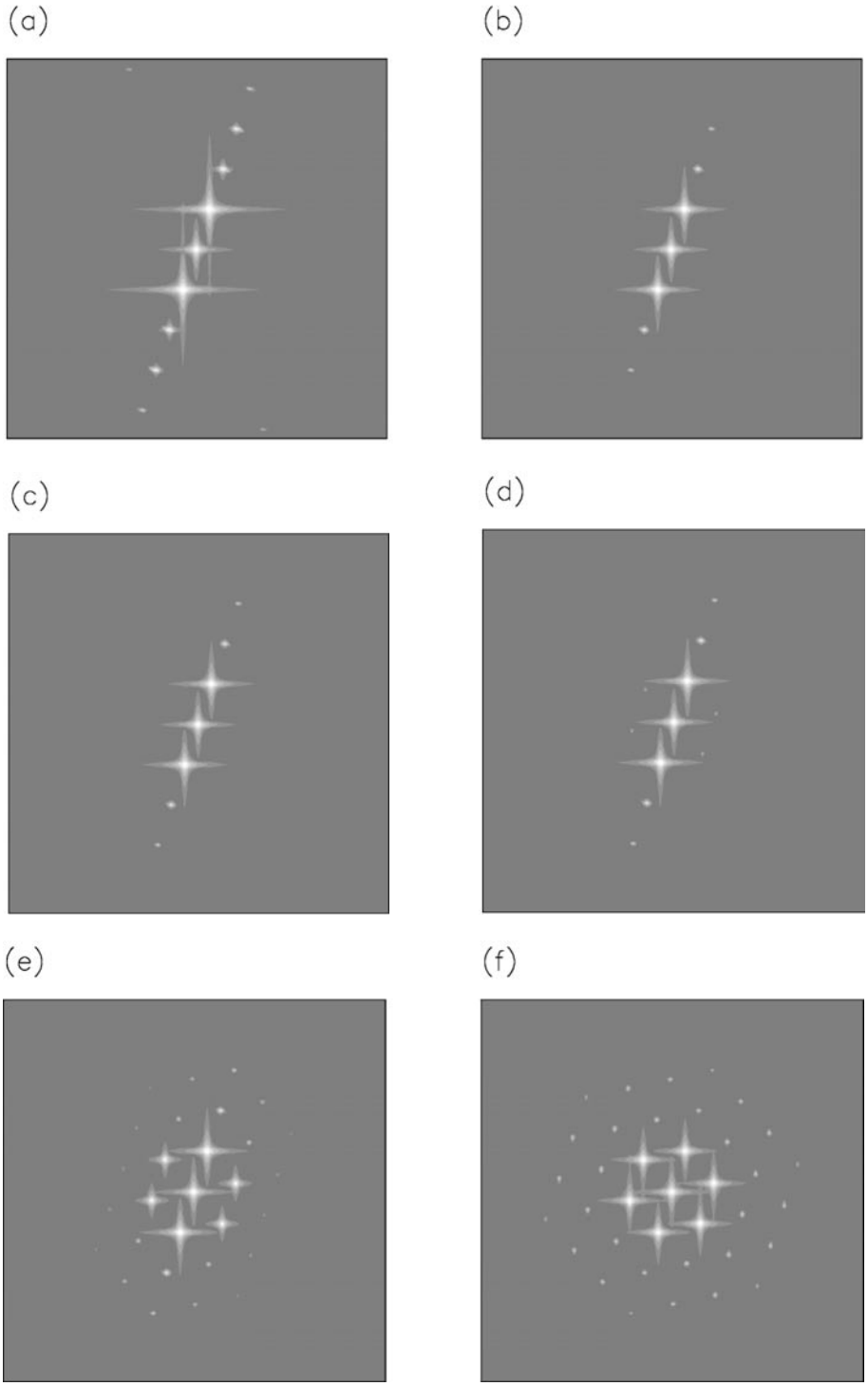

Figure 5. Scattering intensity in the transition from regular lamellar to hexagonal structures. The time is $t = 0$, $13\,000\,\Delta t$, $26\,000\,\Delta t$, $39\,000\,\Delta t$, $52\,000\,\Delta t$ and $65\,000\,\Delta t$ with $\Delta t = 1/45$ from (a) to (f).

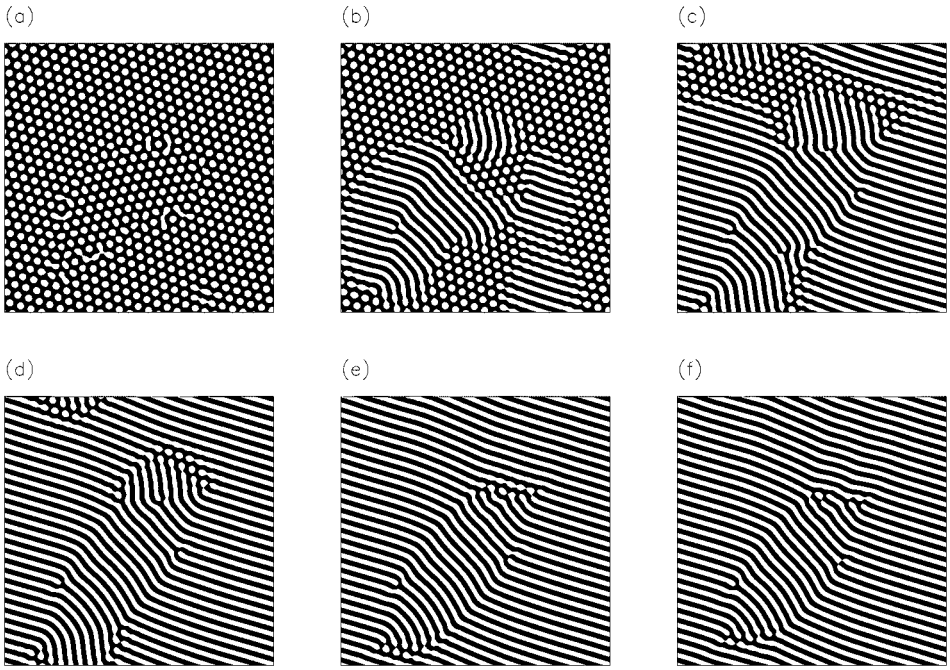

Figure 6. The morphological transition from disordered hexagonal structures with grains to lamellar structures. The time is $t = 0, 20\,000\,\Delta t, 40\,000\,\Delta t, 60\,000\,\Delta t, 80\,000\,\Delta t$ and $100\,000\,\Delta t$ with $\Delta t = 1/45$ from (a) to (f).

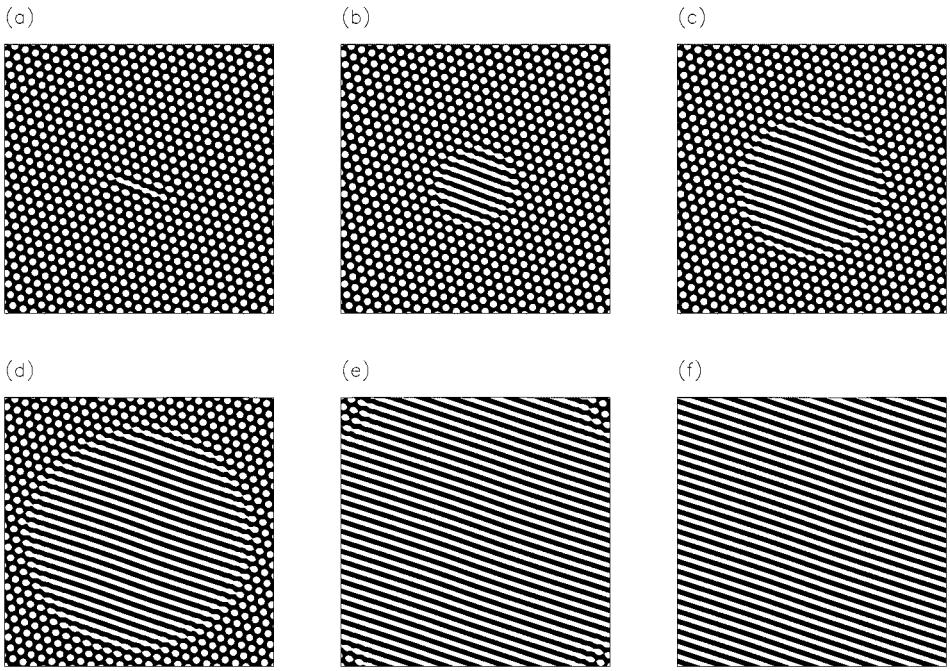

Figure 7. The morphological transition from hexagonal to lamellar structures. Initially a pair of dislocations form the central part of the system. The time is $t = 0$, $15\,000\,\Delta t$, $30\,000\,\Delta t$, $45\,000\,\Delta t$, $60\,000\,\Delta t$ and $75\,000\,\Delta t$ with $\Delta t = 1/45$ from (a) to (f).

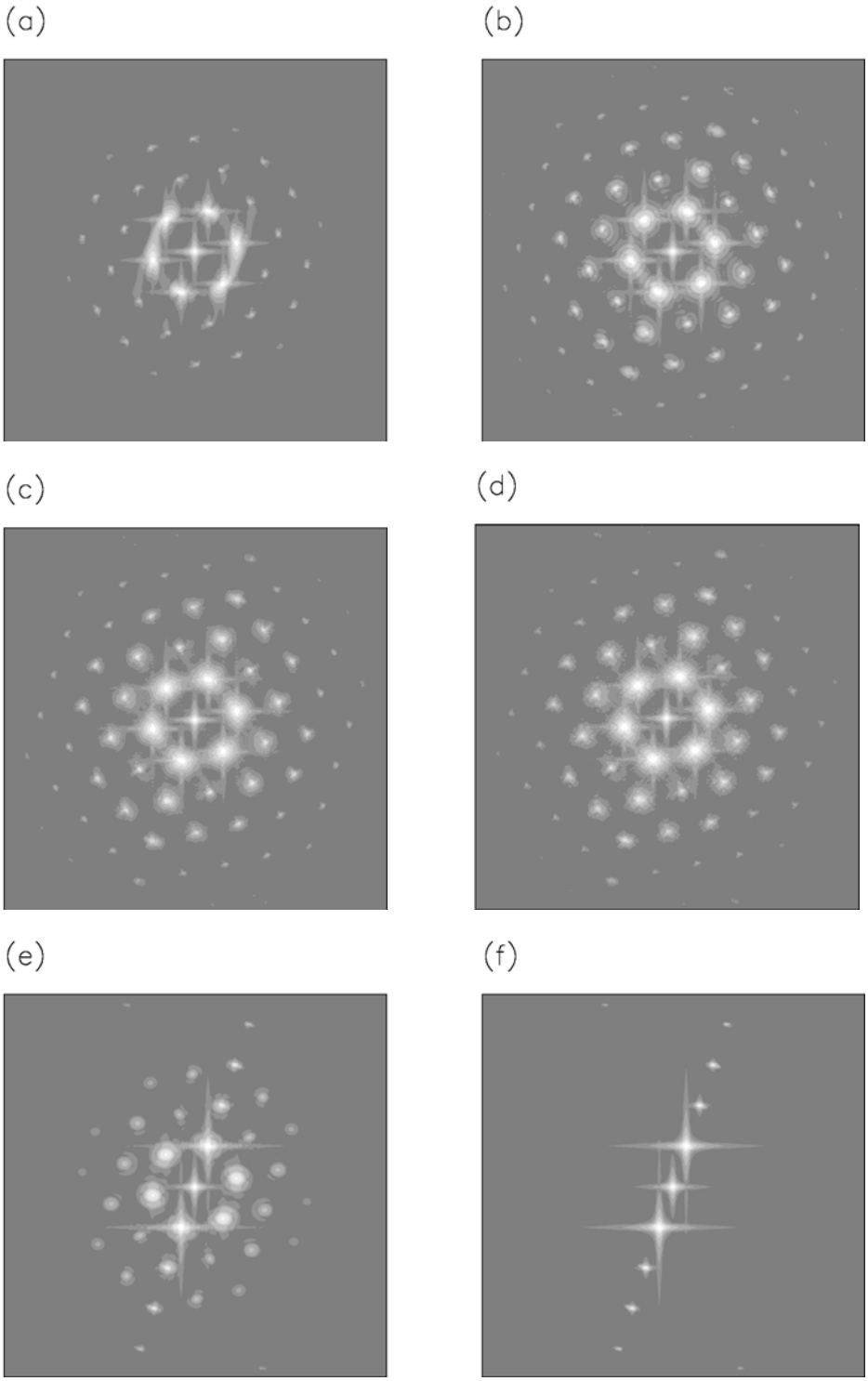

Figure 8. Scattering intensity in the transition shown in figure 7. The time is $t = 0$, $15\,000\,\Delta t$, $30\,000\,\Delta t$, $45\,000\,\Delta t$, $60\,000\,\Delta t$ and $75\,000\,\Delta t$ with $\Delta t = 1/45$ from (a) to (f).

structure emerges along the grain boundaries. Stripe domains nucleated at isolated dislocations also exist, which have a different orientation. However, these lamellar domains are eventually dominated by the major ones. The configuration at the late stage reveals a zigzag pattern influenced by the initial grain boundaries.

In order to investigate systematically the growth of lamellar structures triggered by an isolated defect, we carried out simulations for $\bar{\phi} = 0.04$ which are shown in figure 7. In this case, we put a pair of dislocations initially at the centre of the system. On changing the temperature from $\hat{\tau} = 0.0117$ to $\hat{\tau} = 0.0450$, this defect pair acts as a nucleation centre for the formation of lamellae. In fact, a domain of the lamellar structure grows at the expense of the surrounding hexagonal matrix. It is worth noting that the domain having lamellae takes a hexagonal shape. Furthermore, it is found that there are two kinds of interface depending on the relative orientation of the reciprocal-lattice vectors of lamellar and hexagonal structures, which are equivalent to those in figures 2(a) and 2(b). The scattering intensities at each time step of figure 7 are shown in figure 8. Modulation around the major spots at $t = 15\,000\,\Delta t$ arises from the structure factor of the growing lamellar domain.

We have estimated the velocity ratio of the two boundaries, which is found to be approximately

$$0.93 \leqslant \frac{V_a}{V_b} < 1. \tag{80}$$

The uncertainty is mainly due to the discreteness of domains in which accurate determination of the velocity from the snapshot in figure 7 is difficult. Nevertheless, the theoretical result (79) is found to be not inconsistent with (80).

6. Computer simulations in three dimensions

6.1. From BCC to hexagonal or lamellar structures

Qi and Wang [12, 13] have investigated the kinetics of morphological transitions in three dimensions by solving numerically equation (1) with added random thermal noises. They have studied the transitions by raising the temperature starting from lamellar or hexagonal structures. In this section, we shall show the results of our simulations in three dimensions of transitions from a BCC structure to other mesophases caused by quenching the temperature.

We have solved equation (1) numerically in a cubic system having the mesh number N^3 mainly with $N = 40$. The mesh size is $\Delta x = 1.0$ whereas the time increment is $\Delta t = 0.0756$. The periodic boundary conditions are imposed at the system boundary. We have employed the discretization scheme used in reference [23] for the Laplace operator. The parameters g and α are fixed at $g = 5.45$ and $\alpha = 1.32$. The average volume fraction $\bar{\phi}$ is chosen as $\bar{\phi} = 0.06$ throughout this subsection.

Starting with a random initial condition for ϕ around $\bar{\phi}$, we have provided an equilibrated BCC structure at $\hat{\tau} = 0.0110$, which is shown at the top of figure 9. We have checked the system size dependence of the morphology by changing the mesh number N and found that a BCC structure is actually formed for $N = 32$, 36, 38 and 40 whereas a hexagonal structure appears for $N = 34$ and 37. The result shown below is the case for $N = 40$.

The time evolution of the structure quenched to $\hat{\tau} = 0.0184$ is displayed in figure 9 where the isosurface $\phi = \bar{\phi}$ is drawn. It is evident that the domains along the [111] direction of the BCC structure merge with each other and the hexagonal structure of cylindrical domains is developed. This is consistent with the theoretical results given in section 3 as well as the earlier results [10] and the experiments [1].

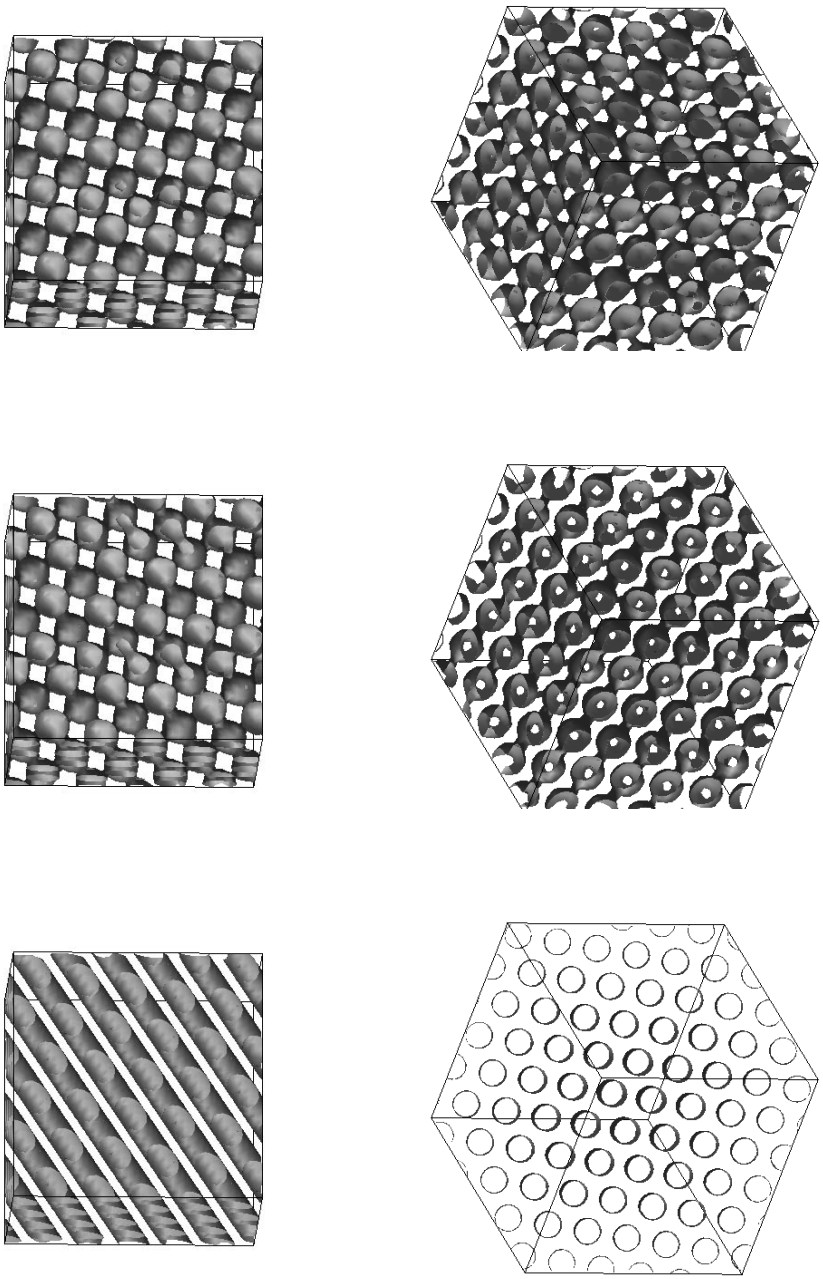

Figure 9. The morphological transition from BCC to hexagonal structures. The left (right) column displays the view from the [100] ([111]) direction of the BCC structure. The time is $t = 0$, $t = 25\,000\,\Delta t$ and $t = 30\,000\,\Delta t$ with $\Delta t = 0.0756$ from the top to the bottom.

If the system is quenched to a lower temperature $\hat{\tau} = 0.0317$, a percolated lamellar structure [13] emerges in the intermediate time step and then it evolves to a final hexagonal state as is shown in figure 10. In the quench to $\hat{\tau} = 0.0450$, a similar percolated lamellar structure appears and it exists within our simulation time. However, this does not mean that

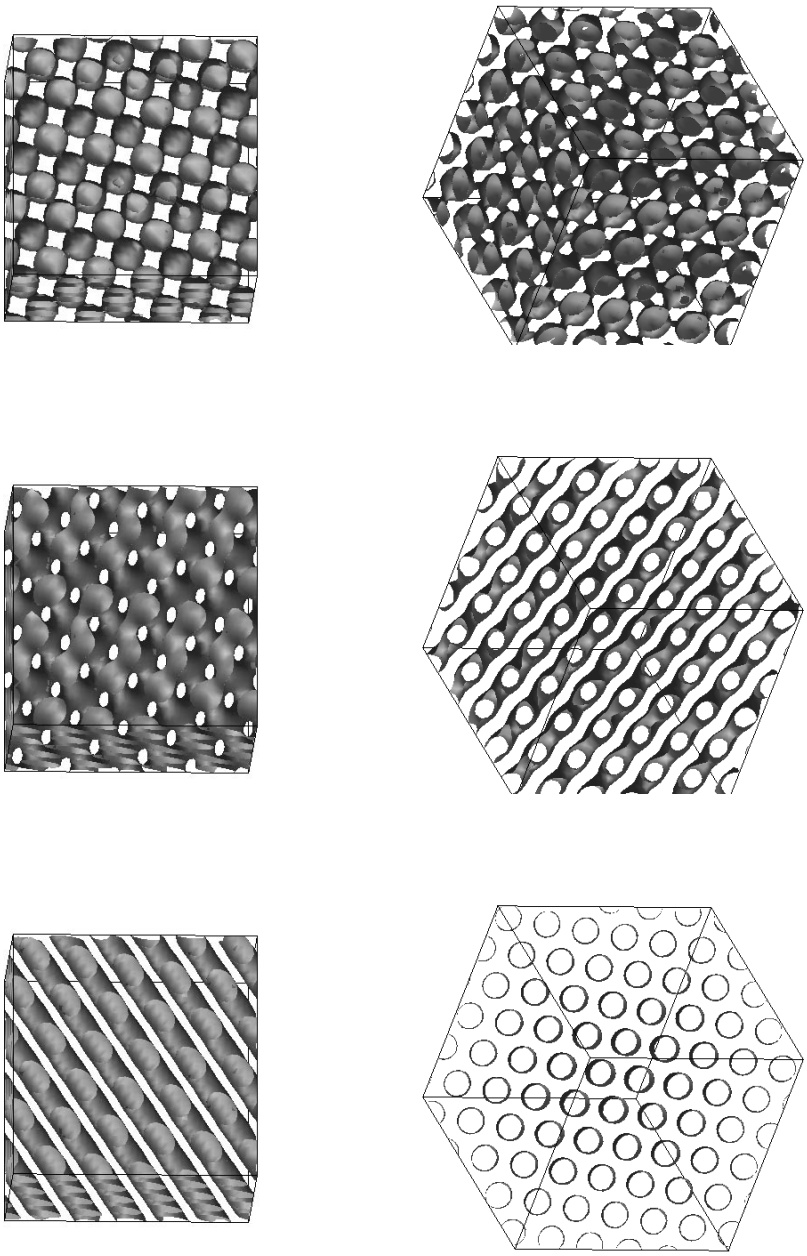

Figure 10. The morphological transition from BCC to hexagonal structures via a percolated lamellar structure. The left (right) column displays the view from the [100] ([111]) direction of the BCC structure. The time is $t = 0$, $t = 5000\,\Delta t$ and $t = 6000\,\Delta t$ with $\Delta t = 0.0756$ from the top to the bottom.

the percolated lamellar structure is thermodynamically stable state since the thermal random force is not added in the present simulations and the system size is rather small. When we make a deep quench to $\hat{\tau} = 0.1784$, the BCC morphology is transformed to a lamellar structure via a percolated lamellar structure. This is shown in figure 11.

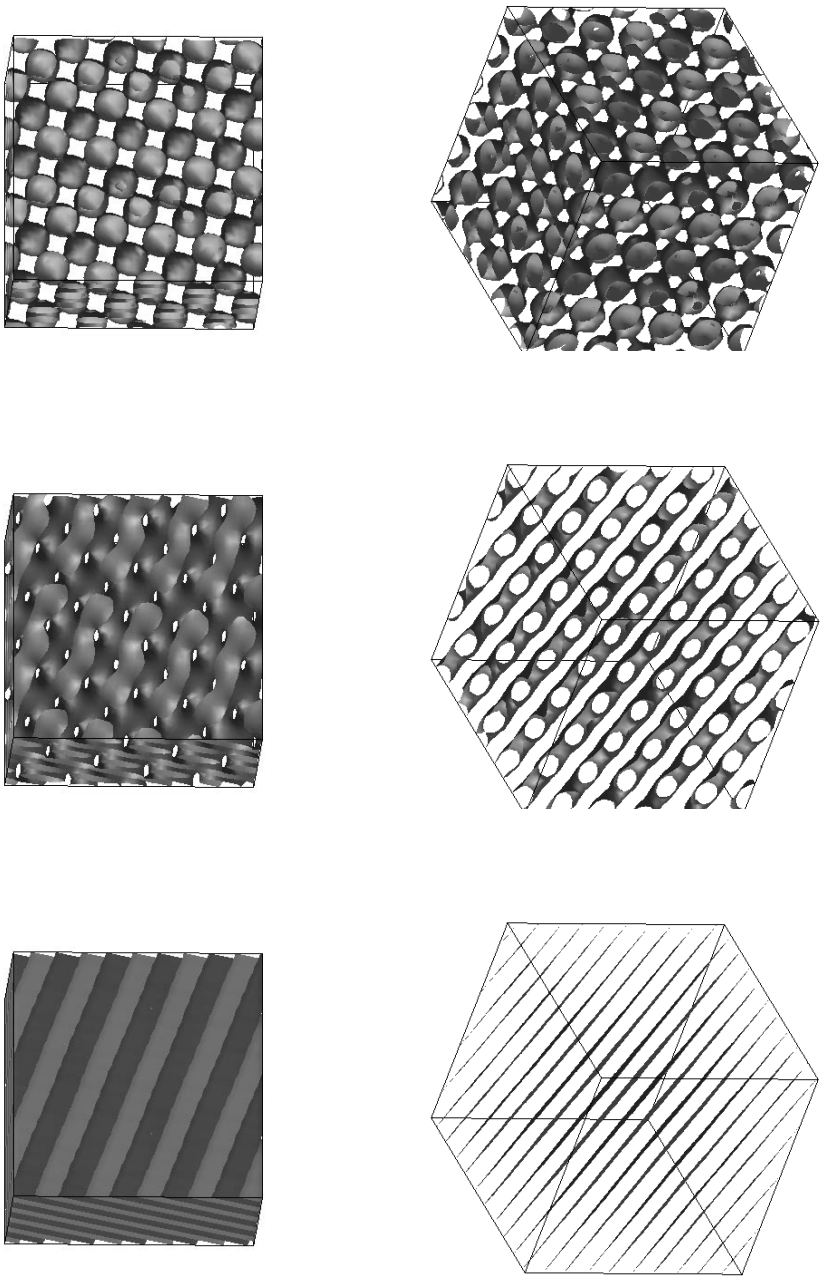

Figure 11. The morphological transition from BCC to lamellar structures. The left (right) column displays the view from the [100] ([111]) direction of the BCC structure. The time is $t = 0$, $t = 500\,\Delta t$ and $t = 1500\,\Delta t$ with $\Delta t = 0.0756$ from the top to the bottom.

Although it is not shown in the figure, it is also observed in a different run that two lamellar domains whose normal vectors are oriented in the $(1, 0, 1)$ and $(1, 1, 0)$ directions are formed, divided by a grain boundary, and then one of the lamellae becomes dominant quite slowly.

6.2. Bicontinuous structure

In this subsection, we describe a new bicontinuous structure found by computer simulations. When $\bar{\phi} = 0.04$, a curious structure, as shown in figure 12, is formed in the interval $0.035 \leqslant \hat{\tau} \leqslant 0.042$ starting with a random initial condition for ϕ. The meaning of the colours is as follows. The ϕ-rich side ($\phi > \bar{\phi}$) of the isosurface $\phi = \bar{\phi}$ is shown in blue whereas the side where $\phi < \bar{\phi}$ is shown in red. Each part of figure 12 shows a different perspective. It is noted that three tube-like domains meet at a vertex.

In order to examine the system size dependence, we have carried out simulations by changing N from $N = 32$ to $N = 40$. When $N = 34$, a lamellar structure appears. For other values of N, we have neither lamellar nor hexagonal structures, but a bicontinuous one emerges. Although it is not perfectly periodic, the local structure is essentially the same as in figure 12 (where $N = 32$ and $\hat{\tau} = 0.0383$). Therefore we believe that this is intrinsic, not forced by the special ratio of the system size to the period of modulation.

The structure in figure 12 is different from the gyroid observed experimentally [17]. In order to clarify the bicontinuous structure, we have evaluated the scattering intensity which has the following main peaks (in units of $2\pi/N$ apart from the origin $\mathrm{O} = (0, 0, 0)$): $\mathrm{A} = (5, -3, 0)$, $\mathrm{B} = (3, -5, -1)$, $\mathrm{C} = (2, -2, -5)$, $\mathrm{D} = (4, 0, -4)$, $\mathrm{E} = (3, -1, 5)$, $\mathrm{F} = (1, 5, -3)$ and $\mathrm{G} = (4, 4, 2)$. The intensities of peaks A, B, C and D are the almost same; these are normalized to unity. The relative intensity of the peaks E and F is about 0.25 and that of G is about 0.2. Note that peak G can be generated by E and F as $\overrightarrow{\mathrm{OE}} + \overrightarrow{\mathrm{OF}} = \overrightarrow{\mathrm{OG}}$ and hence hereafter we will not consider it.

It is an easy task to show that the points O, E, A and C are on the same plane. The points O, A and C constitute an almost proper triangle with the side lengths $\sqrt{33}$, $\sqrt{34}$ and $\sqrt{35}$. This implies that there is a hexagonal structure of cylindrical domains whose axis is normal to the plane OEAC.

It is also interesting to see that the points O, F, B and D form a diamond shape with each side length $\sqrt{35}$. Thus there is a slightly distorted hexagonal structure normal to the OFBD plane. Note that the points A, B, C and D form a parallelogram with the length $\mathrm{AB} = \mathrm{CD} = 3$ and $\mathrm{BC} = \mathrm{DA} = \sqrt{26}$. The angle between the two vectors $\overrightarrow{\mathrm{BD}}$ and $\overrightarrow{\mathrm{AC}}$ is close to $\pi/3$. From these properties, we deduce that the bicontinuous structure is a superposition of an almost proper hexagonal structure and a distorted one having different orientations. We cannot state conclusively at present whether the structure is really in thermodynamic equilibrium or not since the system size is small and the thermal fluctuation is not taken into account in the present simulations.

We make the remark that Saeki *et al* [24] have also found the same bicontinuous structure as in figure 12 by computer simulations of (1). They have employed an entirely different numerical algorithm. Furthermore, they [25] claim that the structure is identical with the metastable phase in the lamellar–gyroid transition observed in scattering experiments on water–surfactant mixtures [6]. These findings provide further support for the result shown here not being an artifact.

7. Summary and discussion

We have presented a coarse-grained approach in terms of the amplitudes of modulated structures to derive the stability limit of each mesophase and the interface velocity of a growing structure. The results are compared with those of computer simulations. The velocity ratio obtained is qualitatively in agreement with simulations. However, since the interfacial energy is estimated using a rather rough approximation, a more refined theory is necessary to make a quantitative comparison.

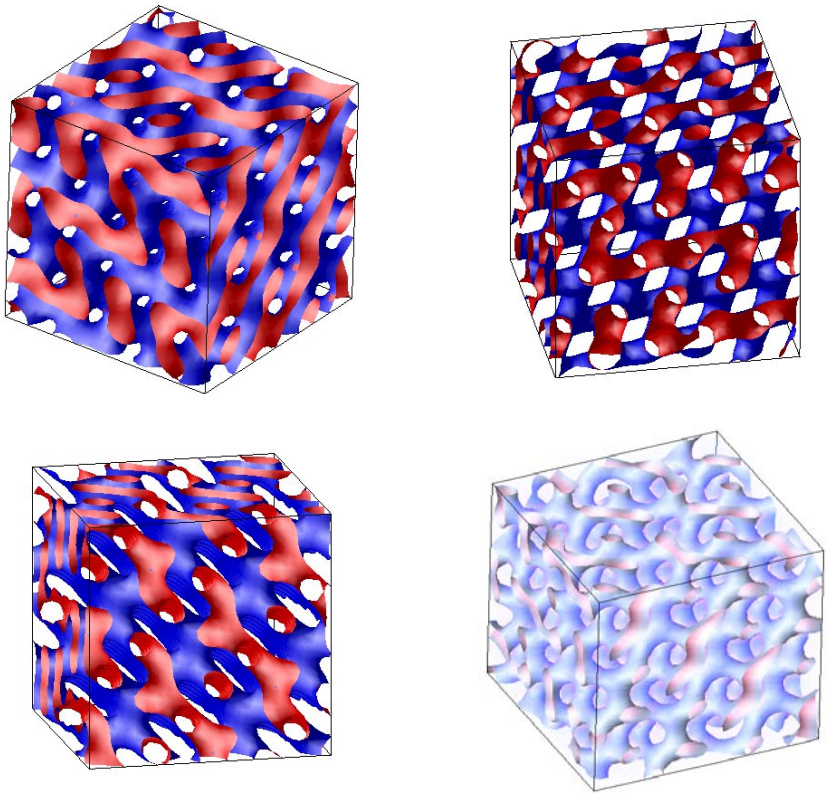

Figure 12. Bicontinuous structure for $\hat{\tau} = 0.0383$ and $\bar{\phi} = 0.04$ at $t = 300\,000\,\Delta t$ with $\Delta t = 0.0756$ starting from a random configuration of ϕ. The figures shown in red and blue are the views from three different directions with the isosurface $\phi = \bar{\phi}$. For comparison, the figure bottom right shows the concentration variation with the isosurface $\phi = -0.1$.

In two-dimensional simulations, we have shown that the grain boundaries or dislocations play a decisive role for the kinetics of morphological transitions. In three dimensions, transitions from BCC to hexagonal or lamellar structures are investigated where we have found that a percolated lamellar structure appears at the intermediate stage of evolution unless the quench from the BCC state is not sufficiently small.

The present results in three dimensions are only qualitative. This is because we are mainly concerned with the domain evolution—such as deformation and merging during the order–order transitions. We emphasize that this kind of study is necessary to get insight into the morphological change of domains and to develop a dynamic theory tractable analytically beyond the simple linear stability argument. If one wishes to investigate quantitatively the kinetics of transitions, the degree of the structural change from references [12, 13] and the various morphological measures such as the Euler characteristics, and mean and Gaussian curvatures [27, 28] would be useful.

A new bicontinuous structure is obtained in simulations and the symmetry property of the structure is analysed using the scattering intensity. As mentioned in section 6, Imai *et al* have found this bicontinuous structure experimentally between lamellar and gyroid phases in water–surfactant mixtures [6, 25]. By analysing the x-ray scattering intensities, they conclude that the structure belongs to the $R\bar{3}c$ symmetry group. (In their earlier paper [6],

they identified it erroneously as $R\bar{3}m$ symmetry.) We have verified (though not shown in figures) that the first four or five scattering peaks of the angle-averaged Fourier transform of our bicontinuous structure are indeed consistent with the $R\bar{3}c$ symmetry. It is mentioned (though somewhat confusing) that a very similar bicontinuous structure has been found experimentally in spinodal decomposition of a polymer blend [26]. Application of the morphological measures in reference [29] to these structures would also be interesting.

In the present simulations in three dimensions, we have employed the discretization scheme from reference [23] which has been confirmed empirically to be the most efficient for minimizing the anisotropy of the underlying cells. However, the discretization method was designed originally to apply to spinodal decomposition where domains grow indefinitely. Therefore one needs to proceed with caution when using it to investigate the order–order transition. We have examined the robustness of the rhombohedral structure by changing the system size in section 6 and have checked recently that it appears even for the system size $64 \times 64 \times 64$ [30]. Furthermore, as mentioned in the preceding section, Saeki *et al* [24] have obtained the same structure independently by using a different numerical method, adding a random force. From these facts, we believe that the bicontinuous structure is an intrinsic one, free from the possible deficiencies of the simulation scheme.

What we have not considered in the present paper is the elastic effect due to weak deformation of the mesophases. In other words, we have ignored the phase variable in the amplitude equation. This is justified when the structural mismatch is small as in figures 2. However, the elasticity is generally important in the kinetics of order–order transitions, especially when grain boundaries and dislocations are present. We will present a dynamic theory of morphological transitions considering both the amplitude and the phase elsewhere in the near future.

Acknowledgments

We are grateful to H Hasegawa, M Imai, R Kobayashi, T Koga and Y Oono for valuable discussions and useful advice on computer simulations. This work was supported by a Grant-in-Aid from the Ministry of Education, Science and Culture of Japan.

Appendix

Here we derive the effective free energy for a hexagonal mesophase in terms of the complex amplitudes. First, let us consider the local part $W(\phi)$ in (3). Substituting

$$\phi(\vec{r}) = c + \sum_{i=1,2,3} [H_i(\vec{r}, t)\mathrm{e}^{\mathrm{i}\vec{Q}_i\cdot\vec{r}} + H_i^*(\vec{r}, t)\mathrm{e}^{-\mathrm{i}\vec{Q}_i\cdot\vec{r}}] \tag{A.1}$$

into $W(\phi)$, one obtains

$$\begin{aligned} W_{eff}(H_i) = \sum_{i=1,2,3} [3gc^2|H_i|^2 + \frac{3g}{2}|H_i|^4] + 6g(|H_1|^2|H_2|^2 + |H_2|^2|H_3|^2 + |H_3|^2|H_1|^2) \\ + 6cg(H_1H_2H_3 + H_1^*H_2^*H_3^*) \end{aligned} \tag{A.2}$$

where the term proportional to τ is excluded; it is considered together with the nonlocal part.

The nonlocal part of the free energy can be written in terms of the Fourier components as

$$\frac{1}{2}\int \frac{\mathrm{d}\vec{q}}{(2\pi)^3}\,\Gamma(q)\phi_{\vec{q}}\phi_{-\vec{q}} \tag{A.3}$$

where $\Gamma(q) = q^2 - \tau + \alpha/q^2$. The Fourier transform of (A.1) is given by

$$\phi_{\vec{q}} = \sum_{i=1,2,3} \int \mathrm{d}\vec{r}\, [H_i(\vec{r},t)\mathrm{e}^{\mathrm{i}\vec{Q}_i\cdot\vec{r}} + H_i^*(\vec{r},t)\mathrm{e}^{-\mathrm{i}\vec{Q}_i\cdot\vec{r}}]\mathrm{e}^{-\mathrm{i}\vec{q}\cdot\vec{r}}$$
$$= \sum_{i=1,2,3} (H_{i,\vec{q}-\vec{Q}_i} + H^*_{i,\vec{q}+\vec{Q}_i}). \tag{A.4}$$

From (A.3) and (A.4), one obtains, omitting the higher harmonics,

$$\frac{1}{2}\int \frac{\mathrm{d}\vec{p}}{(2\pi)^3} \sum_{i=1,2,3} [\Gamma(\vec{Q}_i + \vec{p}) + \Gamma(\vec{Q}_i - \vec{p})] H_{i,\vec{p}} H^*_{i,-\vec{p}}. \tag{A.5}$$

Expansion of $\Gamma(\vec{Q} \pm \vec{p})$ in powers of $\vec{p}$ yields

$$\Gamma(\vec{Q} + \vec{p}) + \Gamma(\vec{Q} - \vec{p}) = 2\Gamma(Q) + \sum_{\alpha,\beta} p^\alpha p^\beta \frac{\partial^2 \Gamma}{\partial Q^\beta\, \partial Q^\alpha} + \cdots. \tag{A.6}$$

Since

$$\frac{\partial^2\Gamma}{\partial Q^\beta\, \partial Q^\alpha} = \delta_{\alpha\beta}\frac{1}{Q}\frac{\partial\Gamma}{\partial Q} + Q^\alpha Q^\beta \frac{1}{Q}\frac{\partial}{\partial Q}\left(\frac{1}{Q}\frac{\partial\Gamma}{\partial Q}\right) \tag{A.7}$$

and $\partial\Gamma/\partial Q = 0$ for the equilibrium value of Q, we finally obtain the effective free energy

$$F_{eff}\{H_i\} = \int \mathrm{d}\vec{r}\left[c_0 \sum_i |\vec{Q}_i \cdot \vec{\nabla} H_i|^2 + W_{eff}(H_i)\right] \tag{A.8}$$

where c_0 has been defined in (64).

If one makes the approximation that ∇^2 in equation (1) can be replaced by $-Q^2$, the kinetic equation for the amplitudes is given by

$$\frac{\partial H_i}{\partial t} = -Q^2 \frac{\delta F_{eff}}{\delta H_i^*}. \tag{A.9}$$

When H_i is real, one may put $H_i = H_i^*$ after taking the functional derivative in (A.9). The result agrees with (62).

References

[1] Kimishima K, Koga T and Hashimoto T 2000 *Macromolecules* **33** 968
[2] Sakamoto N and Hashimoto T 1998 *Macromolecules* **31** 8493
[3] Krishnamoorti R, Modi M A, Tse M F and Wang H-C 2000 *Macromolecules* **33** 3803
Krishnamoorti R, Modi M A, Tse M F and Wang H-C 2000 *Macromolecules* **33** 3810
[4] Mortensen K, Kleppinger R, Theunissen E and Reynaers H 2001 *J. Phys.: Condens. Matter* **13** 5731
[5] Imai M, Nakaya K and Kato T 1999 *Phys. Rev.* E **60** 734
[6] Imai M, Kawaguchi A, Saeki A, Nakaya K, Kato T, Ito K and Amemiya Y 2000 *Phys. Rev.* E **62** 6865
[7] Matsen M W and Schick M 1994 *Phys. Rev. Lett.* **72** 2660
[8] Matsen M W and Bates F S 1996 *Macromolecules* **29** 7641
Matsen M W and Bates F S 1996 *Macromolecules* **29** 1091
[9] Shi A, Noolandi J and Desai R C 1996 *Macromolecules* **29** 6487
[10] Laradji M, Shi A, Desai R C and Noolandi J 1997 *Phys. Rev. Lett.* **78** 2577
[11] Laradji M, Shi A, Noolandi J and Desai R C 1997 *Macromolecules* **30** 3242
[12] Qi S and Wang Z-G 1996 *Phys. Rev. Lett.* **76** 1679
[13] Qi S and Wang Z-G 1997 *Phys. Rev.* E **55** 1682
[14] Goveas J L and Milner S T 1997 *Macromolecules* **30** 2605
[15] Cross M C and Hohenberg P C 1993 *Rev. Mod. Phys.* **65** 851
[16] Chen L-Y, Goldenfeld N, Oono Y and Paquette G 1994 *Physica* A **204** 111
[17] Hajduk D A, Harper P E, Gruner S M, Honeker C C, Kim G, Thomas E L and Fetters L J 1994 *Macromolecules* **27** 4063

[18] Bahiana M and Oono Y 1990 *Phys. Rev.* A **41** 6763
[19] Ohta T and Kawasaki K 1986 *Macromolecules* **19** 2621
Ohta T and Kawasaki K 1990 *Macromolecules* **23** 2413
[20] Seul M and Andelman D 1995 *Science* **267** 476
[21] Fredrickson G H and Helfand E 1987 *J. Chem. Phys.* **87** 697
[22] Tsori V, Andelman D and Schick M 2000 *Phys. Rev.* E **61** 2848
[23] Shinozaki A and Oono Y 1993 *Phys. Rev.* E **48** 2622
[24] Saeki A *et al* 2001 in preparation
[25] Imai M *et al* 2001 private communication
[26] Ribbe A E and Hashimoto T 1997 *Macromolecules* **30** 3999
[27] Gozdz W T and Holyst R 1996 *Phys. Rev.* E **54** 5012
[28] Holyst R and Gozdz W T 1997 *J. Chem. Phys.* **106** 4773
[29] Fialkowski M, Aksimentiev A and Holyst R 2001 *Phys. Rev. Lett.* **86** 240
[30] Nonomura M and Ohta T 2001 *Physica* A submitted